CHALMERS
UNIVERSITY OF TECHNOLOGY

A stabilized P1 domain decomposition finite element method for time harmonic Maxwell's equations

Citation for the original published paper (version of record):
Asadzadeh, M., Beilina, L. (2023). A stabilized P1 domain decomposition finite element method for time harmonic Maxwell's equations. Mathematics and Computers in Simulation, 204: 556-574. http://dx.doi.org/10.1016/j.matcom.2022.08.013

Available online at www.sciencedirect.com
ScienceDirect
Mathematics and Computers in Simulation 204 (2023) 556–574
MATHEMATICS AND COMPUTERS IN SIMULATION
www.elsevier.com/locate/matcom

Original articles

A stabilized $P1$ domain decomposition finite element method for time harmonic Maxwell's equations

M. Asadzadeh, L. Beilina*

Department of Mathematical Sciences, Chalmers University of Technology and University of Gothenburg, SE-412 96, Gothenburg, Sweden

Received 25 August 2020; received in revised form 19 January 2022; accepted 12 August 2022
Available online 31 August 2022

Abstract

One way of improving the behavior of finite element schemes for classical, time-dependent Maxwell's equations is to render their hyperbolic character to elliptic form. This paper is devoted to the study of a stabilized linear, domain decomposition, finite element method for the time harmonic Maxwell's equations, in a dual form, obtained through the Laplace transformation in time. The model problem is for the particular case of the dielectric permittivity function which is assumed to be constant in a boundary neighborhood. The discrete problem is coercive in a symmetrized norm, equivalent to the discrete norm of the model problem. This yields discrete stability, which together with continuity guarantees the well-posedness of the discrete problem, cf Arnold et al. (2002) [3], Di Pietro and Ern (2012) [45]. The convergence is addressed both in *a priori* and *a posteriori* settings. In the a priori error estimates we confirm the theoretical convergence of the scheme in a L_2-based, gradient dependent, triple norm. The order of convergence is $\mathcal{O}(h)$ in weighted Sobolev space $H^2_w(\Omega)$, and hence optimal. Here, the weight $w := w(\varepsilon, s)$ where ε is the dielectric permittivity function and s is the Laplace transformation variable. We also derive, similar, optimal a posteriori error estimates controlled by a certain, weighted, norm of the residuals of the computed solution over the domain and at the boundary (involving the relevant jump terns) and hence independent of the unknown exact solution. The a posteriori approach is used, e.g. in constructing adaptive algorithms for the computational purposes, which is the subject of a forthcoming paper. Finally, through implementing several numerical examples, we validate the robustness of the proposed scheme.

Keywords: Time harmonic Maxwell's equations; P_1 finite elements; Stability; A priori estimate; A posteriori estimate; Convergence

1. Introduction

Because of the growing efficiency of computing facilities, constructing efficient computational methods for simulation of partial differential equations, in two and three dimensions, has become a reality. This is of vital importance and becomes more apparent in industrial applications, e.g. when the computational domain is very large. In particular, nowadays there are a lot of industrial applications in subsea and subsurface imaging where the computational domains comprise very large subdomains with constant values of material parameters on each subdomain. Usually, only some part of these domains, where there is an over-admissible material change, presents extra caution and therefore is of interest. Such phenomena are modeled, e.g. in equations possessing

* Corresponding author.
E-mail addresses: mohammad@chalmers.se (M. Asadzadeh), larisa.beilina@chalmers.se (L. Beilina).

https://doi.org/10.1016/j.matcom.2022.08.013

constant material parameters in a boundary neighborhood of a significant part of the computational domain. Some applications of the Maxwell's models, describing the electro-magnetic fields, fit well into this category.

As in the realm of finite elements: it is well known that for the stable implementations of the finite element solution for the Maxwell's equations divergence-free edge elements are the most advantageous choice from a theoretical point of view, see, e.g. [40,43]. Recently, in [26], a second order method with mass lumping was applied for approximation of Maxwell's equations in time domain using $H(curl)$ conforming finite elements. Also divergence-free edge elements for approximation of Maxwell's equations are used in combination with other methods, see [7,21,27,46]. But the edge elements are less attractive for numerical solution since they are too expensive to implement. On the contrary, continuous P1 finite elements provide efficiently implemented non-expensive solution of Maxwell's equations compared to $H(curl)$ conforming methods, see, e.g. [8,19,34]. In particular, the advantage of the P1 approach is apparent for the case considered in the current work when the dielectric permittivity function is a constant in a boundary neighborhood. This phenomenon is verified through numerical simulations for time-dependent Maxwell's equations in [8,10,11]. Furthermore, P1 schemes can be efficiently used in a fully explicit finite element scheme with lumped mass matrix as in [10,28,39]. However, applied to the solution of Maxwell's equations, P1 elements have a number of drawbacks, e.g. in domains with re-entrant corners and non-zero tangential components at the boundary, they result in spurious oscillatory solutions [41,44]. Different techniques are used to correctly represent field singularities at re-entrants, e.g. the singular field method [14]. A number of other techniques, which focus on removing oscillatory behavior from the numerical approximations of Maxwell's equations, are given, e.g. in [35–37,42], and [44].

We circumvent such difficulties considering convex computational domains with constant values of parameters in a boundary neighborhood. More specifically, in this work we consider continuous stabilized P1, domain decomposition, finite element method for the numerical solution of time harmonic Maxwell's equations for the special case when the dielectric permittivity function has a constant value in a boundary neighborhood. In this way the Maxwell's equations are transformed to a set of time-independent wave equations on the boundary neighborhood with several adequate boundary conditions that can be handled by the P1 finite element approach.

Recently, stability and consistency of the stabilized P1 finite element method for time-dependent Maxwell's equations were presented in [10] and a, related, short communication [11]. Efficiency in using explicit P1 finite element schemes is evident for solution of *Coefficient Inverse Problems* (CIPs). In many algorithms, for electromagnetic CIPs, a qualitative collection of experimental data (measurements) is necessary at the boundary of the computational domain to determine the dielectric permittivity function inside it, whereas the numerical solutions for time-dependent Maxwell's equations are required in the entire space $\mathbb{R}^3$, see, e.g. [9,12,13,48], and [49]. In such cases it is efficient to consider Maxwell's equations with constant dielectric permittivity function in a neighborhood of the boundary of a relevant computational domain. In this regard, an explicit P1 finite element scheme in non-conductive media is numerically tested for solution of time-dependent Maxwell's system in 2D and 3D cases in [8]. The P1 finite element scheme of [8] is used for solution of different CIPs, where the objective is to determine the dielectric permittivity function in non-conductive media for time-dependent Maxwell's equations using simulated and experimentally generated data, see, e.g. [9,12,13], and [48,49].

In the present study we are using the Laplace transform to obtain time-harmonic model problem which, hopefully, will have further applications in deriving algorithms for solution of CIPs. Thus, the convergence analysis of this note can be important for future investigations. The Laplace transform is more convenient and easier, compared to Fourier transform, since it keeps the problem in real space. Note that the Laplace transform is already applied in different algorithms for solution of CIPs: in [9] the Laplace transform was applied to the time-dependent wave equation, with the transform parameter s as the pseudo-frequency. Then the globally convergent method for reconstruction of the wave speed function in the resulting time-harmonic equation was derived in a pseudo-frequency interval: with $s \in [\underline{s}, \bar{s}]$. The method of [9] was further tested on experimental data in [48,49], and the references therein.

In this study we derive optimal a priori and a posteriori convergence rates for the P1 finite element scheme, for the time harmonic Maxwell system, assuming a constant dielectric permittivity function at a boundary neighborhood, hence with no in- and outflow. The Neumann type problem is well-conditioned due to the fact that the time-harmonic Maxwell's equations are elliptic, whereas the original time-dependent Maxwell's equations are hyperbolic. An a priori approach has been considered by several authors in different settings, where some classical studies are, e.g. the work [19] on continuous Galerkin for time dependent problem in 3D, and quasi-interpolation as well as edge finite element for low regularity solutions by [31,32], respectively. Our a posteriori approach for

the time harmonic Maxwell's equations, adopted to P1, possesses jump terms at interelement boundaries, hence sought for discontinuous Galerkin-like treatment. There are many results for the a posteriori error estimates for the classical time dependent Maxwell's equations, e.g. [20] is addressing the robustness issue, a general work on error estimations is given in [47], and in [25] the authors consider hp-adaption. There are many other studies relevant to this work, e.g. in [18], the augmented formulations are derived, [22,23], and [24] are raising the issues as coercivity, singularities and weighted regularization in polyhedral domains. In [34] the continuous Galerkin is studied for the Maxwell's equations. But there are far less P1 a posteriori studies in the time-harmonic case for the non-constant dielectric permittivity function. In our knowledge, a rigorous *a priori* and *a posteriori* FEM analyses with varying dielectric permittivity function are missing for time-harmonic Maxwell's equations, and this work fills the gap.

An outline of this paper is as follows. In Section 2 we introduce the mathematical model and present the problem for the time harmonic Maxwell's equations, where we assumed no dielectric volume charge. In Section 3 we describe the structure of domain decomposition. Section 4 concerns the study of variational problem for the stabilized model, set up of the finite element scheme and a proof for its well-posedness. Section 5 is devoted to the error analysis, where optimal a priori and a posteriori error estimates are derived in a, gradient dependent, triple norm of Sobolev type (which, under certain assumptions, can be made equivalent to H^1-norm). In the a posteriori case the boundary residual, containing a normal derivative, is balanced by a multiplicative power of the mesh parameter. Finally, our concluding Section 6 is devoted to numerical implementations that justify the robustness of the theoretical results and the efficiency of approximations.

Throughout the paper C denotes a generic constant, not necessarily the same at each occurrence and independent of the mesh parameter, the solution and other involved parameters, unless otherwise specifically specified.

2. The mathematical model

The original model here is given in terms of the electric field $\hat{E}(x,s), x \in \mathbb{R}^d, d = 2,3$ and is varying with the pseudo-frequency $s > const. > 0$, and under the assumption that the magnetic permeability of the medium is $\mu \equiv 1$. We consider the Cauchy problem for the time-harmonic Maxwell's equations for electric field $\hat{E}(x,s)$ assuming vanishing electric volume charges. Hence, the corresponding equation is:

$$\begin{aligned} s^2\varepsilon(x)\hat{E}(x,s) + \nabla\times\nabla\times\hat{E}(x,s) &= s\varepsilon(x)f_0(x), \quad x\in\mathbb{R}^d, \quad d=2,3 \\ \nabla\cdot(\varepsilon(x)\hat{E}(x,s)) &= 0. \end{aligned} \tag{2.1}$$

Here, $\varepsilon(x) = \varepsilon_r(x)\varepsilon_0$ is the dielectric permittivity function, $\varepsilon_r(x)$ is the dimensionless relative dielectric permittivity and ε_0 is the permittivity of the free space. Further

$$\nabla\times\nabla\times E = \nabla(\nabla\cdot E) - \Delta E. \tag{2.2}$$

The Eq. (2.1) is obtained by applying the Laplace transform (in time)

$$\widehat{E}(x,s) := \int_0^{+\infty} E(x,t)e^{-st}dt, \qquad s = const. > 0, \tag{2.3}$$

to the function $E(x,t)$ satisfying the time-dependent Maxwell's equations below

$$\begin{aligned} \varepsilon(x)\frac{\partial^2 E(x,t)}{\partial t^2} + \nabla\times\nabla\times E(x,t) &= 0, \quad x\in\mathbb{R}^d, \ \ d=2,3, \ \ t\in(0,T]. \\ \nabla\cdot(\varepsilon E)(x,t) &= 0, \\ E(x,0) = f_0(x), \quad \frac{\partial E}{\partial t}(x,0) &= 0, \quad x\in\mathbb{R}^d, \quad d=2,3. \end{aligned} \tag{2.4}$$

We note that in the problem (2.4) we take non-zero initial condition $E(x,0) = f_0(x)$ which is important when considering the solution of coefficient inverse problem, in order to determine the function $\varepsilon(x)$ in (2.4) from finite number of observations of the function E at the boundary Γ, and when the problem is reformulated in a bounded domain.

Numerically, it is unrealistic to solve the problem (2.4) in unbounded domains. As adequate computational spatial domain, we consider a convex bounded, polygonal (here axi-parallel rectangular), subdomain $\Omega \subset \mathbb{R}^d$, $d = 2,3$ with boundary Γ. More specifically, let Ω be a simply connected domain. We define $\Omega_2 := \Omega \setminus \Omega_1$, where $\Omega_1 \subset \Omega$ has positive Lebesgue measure and $\partial\Omega \cap \partial\Omega_1 = \emptyset$. In this way, we are cutting out Ω_1 from Ω, the new subdomain

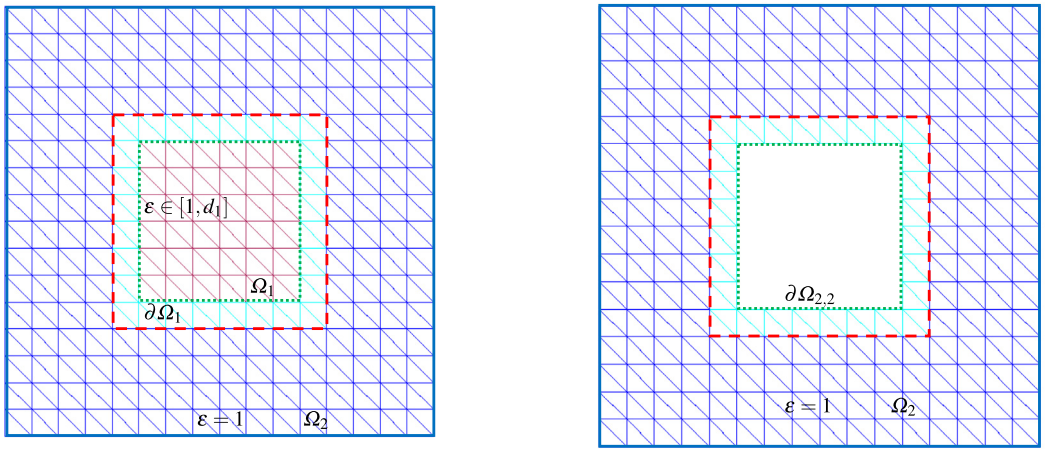

a) $\Omega = \Omega_1 \cup \Omega_2$ b) Ω_2

Fig. 1. Domain decomposition in Ω. The mesh in the domain Ω is a combination of the finite element mesh in Ω_1 outlined in red and light blue color, and the finite element mesh in Ω_2 outlined by blue and light blue color. The mesh in Ω_2 is also presented on b). Meshes in Ω_1 and Ω_2 overlap by the layer of nodes outlined by the light blue color such that they have 2 common inner nodes and boundaries.

Ω_2 shares boundaries with both Ω and Ω_1: $\partial\Omega_2 = \partial\Omega \cup \partial\Omega_1$, $\Omega = \Omega_1 \cup \Omega_2$, $\Omega_1 = \Omega \setminus \Omega_2$ and $\bar{\Omega}_1 \cap \bar{\Omega}_2 = \partial\Omega_1$, (Fig. 1).

To proceed we assume $\varepsilon(x) \in C^2(\mathbb{R}^d)$, $d = 2, 3$ and for a known constant $d_1 > 1$,

$$\begin{aligned} \varepsilon(x) &\in [1, d_1], \qquad \text{for} \quad x \in \Omega_1 = \Omega \setminus \Omega_2, \\ \varepsilon(x) &= 1, \qquad \text{for} \quad x \in \Omega_2 = \Omega \setminus \Omega_1, \end{aligned} \tag{2.5}$$

Remark 1. Conditions (2.5) mean that, in the vicinity of the boundary of the computational domain Ω, Eq. (2.4) transforms to the usual time-dependent wave equation. To derive error bounds, the conditions on the size of ε, play a central role.

In the current work we are using the same set-up for boundaries as in many other works related to the solution of CIPs for Maxwell's equations, see [8,9,12,13]. We use mixed Neumann and first order absorbing boundary conditions, since they provide particular interest from scientific community for solution of applied problems, see [8,12,13] and the references therein, where similar conditions were used.

More specifically, for $\Gamma := \partial\Omega$ the boundary of the computational domain Ω, we use the split $\Gamma = \Gamma_1 \cup \Gamma_2 \cup \Gamma_3$, so that Γ_1 and Γ_2 are the top and bottom sides, with respect to y- (in $2d$) or z-axis (in $3d$), of the domain Ω, respectively, while Γ_3 is the rest of the boundary. Further, $\partial_\nu(\cdot)$ denotes the normal derivative on Γ, where ν is the outward unit normal vector at the boundary Γ.

Remark 2. In most estimates below, it suffices to restrict the Neumann boundary condition for the dielectric permittivity function to: $\partial_\nu \varepsilon(x) = 0$, on $\Gamma_1 \cup \Gamma_2$.

Now, using similar argument as in the studies in [8]–[12], and by Remark 1, for the time-dependent wave equation, we impose first order absorbing boundary condition, see [29], at $\Gamma_1 \cup \Gamma_2$:

$$\partial_\nu E + \partial_t E = 0, \qquad (x, t) \in (\Gamma_1 \cup \Gamma_2) \times (0, T]. \tag{2.6}$$

To impose boundary conditions at Γ_3 we can assume that the surface Γ_3 is located far from the domain Ω_1. Hence, we can assume that $E \approx E^{inc}$ in a vicinity of Γ_3, where E^{inc} is the incident field. Thus, at Γ_3 we may impose Neumann boundary condition

$$\partial_\nu E = 0, \qquad (x, t) \in \Gamma_3 \times (0, T]. \tag{2.7}$$

Finally, using the well known vector-analysis relation (2.2), and applying the Laplace transform to Eq. (2.4) and the boundary conditions (2.6)–(2.7) in the time domain, the problem (2.1) will be transformed to the following model problem

$$\begin{aligned} s^2\varepsilon(x)\hat{E}(x,s) + \nabla(\nabla\cdot\hat{E}(x,s)) - \triangle\hat{E}(x,s) &= s\varepsilon(x)f_0(x), \quad x\in\mathbb{R}^d, d=2,3\\ \nabla\cdot(\varepsilon(x)\hat{E}(x,s)) &= 0,\\ \partial_\nu\hat{E}(x,s) &= 0, \qquad x\in\Gamma_3,\\ \partial_\nu\hat{E}(x,s) &= f_0(x) - s\hat{E}(x,s), \quad x\in\Gamma_1\cup\Gamma_2. \end{aligned} \tag{2.8}$$

3. The structure of domain decomposition

We recall that in the current work we consider the special case when the dielectric permittivity function $\varepsilon(x)$ has a constant value in a boundary neighborhood and satisfies conditions (2.5). These conditions allow to consider different equations in different parts of computational domain, since the Maxwell's equations are transformed to a set of time-independent wave equations on the boundary neighborhood Ω_2.

Hence, instead of solving the model problem (2.8) in the whole domain Ω, we propose to use the domain decomposition method presented below such that the problem (2.8) is solved by FE in the inner domain and the wave equation is computed in the outer domain, see Remark 1. The domain decomposition can be motivated by the fact that in some applications, specially CIPs, (see [9,12,13,48,49]), only a part of the domain can be of interest for investigations, where the dielectric permittivity functions varies in space, and thus, e.g. adaptivity can be applied only in this part. Thus we reduce the computational complexity, and time, for the solution of the whole problem by avoiding the unnecessary computations in the outer domain.

Below we describe the domain decomposition procedure between the two domains Ω_1 and Ω_2 where the FEM is used for computation of the solution of the following problem in Ω_1:

$$\begin{aligned} s^2\varepsilon(x)\hat{E}(x,s) + \nabla(\nabla\cdot\hat{E}(x,s)) - \triangle\hat{E}(x,s) &= s\varepsilon(x)f_0(x), \quad x\in\Omega_1\subset\mathbb{R}^d, d=2,3\\ \nabla\cdot(\varepsilon(x)\hat{E}(x,s)) &= 0,\\ \hat{E}(x,s) &= g, \quad x\in\partial\Omega_1, \end{aligned} \tag{3.9}$$

and another FEM scheme is used in Ω_2 for solution of the wave equation (since $\varepsilon(x)=1$ in Ω_2), after Laplace transformation in time:

$$\begin{aligned} s^2\varepsilon(x)\hat{E}(x,s) - \triangle\hat{E}(x,s) &= s\varepsilon(x)f_0(x), \qquad x\in\Omega_2\subset\mathbb{R}^d, d=2,3\\ \hat{E}(x,s) &= \hat{E}_{\Omega_{2,2}}(x,s), \qquad x\in\partial\Omega_{2,2},\\ \partial_\nu\hat{E}(x,s) &= 0, \qquad x\in\Gamma_3,\\ \partial_\nu\hat{E}(x,s) &= f_0(x) - s\hat{E}(x,s), \quad x\in\Gamma_1\cup\Gamma_2. \end{aligned} \tag{3.10}$$

Communication between Ω_1 and Ω_2 takes place by having the common two-layer inner boundaries with elements outlined by light-blue color, see Fig. 1. The common nodes of both Ω_1 and Ω_2 domains belong to either of the following boundaries (see Fig. 1):

- Nodes on the boundary $\partial\Omega_1$ of Ω_1 (outlined by red dashed line in Fig. 1) are interior nodes for Ω_2,
- Nodes on the inner boundary $\partial\Omega_{2,2}$ of Ω_2 (outlined by green dotted line in Fig. 1) are interior nodes for Ω_1.

By conditions (2.5) function $\varepsilon=1$ at the overlapping nodes between Ω_1 and Ω_2, and thus, both discretization schemes coincide on the common structured overlapping layer, and in this way we avoid instabilities at the interfaces. The domain decomposition scheme is described in the Algorithm 1.

4. Variational approach

We denote the standard inner product in $[L_2(\Omega)]^d$, by $(\cdot,\cdot)$, $d\in\{2,3\}$, and the corresponding norm by $\|\cdot\|$. Similarly we denote by $\langle\cdot,\cdot\rangle_\Gamma$ the standard inner product of $[L_2(\Gamma)]^{d-1}$ and the associated $L_2(\Gamma)$-norm by $\|\cdot\|_\Gamma$. We define the L_2 scalar products

$$(u,v) := \int_\Omega u\cdot v\, d\mathbf{x}, \quad (u,v)_\omega := \int_\Omega u\cdot v\,\omega d\mathbf{x}, \quad \langle u,v\rangle_\Gamma := \int_\Gamma u\cdot v\, d\sigma,$$

Algorithm 1 Domain decomposition algorithm.

1: Solve the problem (3.9) using FEM on the FE mesh in Ω_1.
2: Solve the problem (3.10) using FEM on the FE mesh in Ω_2.
3: Copy FE solution obtained at the boundary $\partial\Omega_{2,2}$ by solving the problem (3.9) in Ω_1 at the Step 1, as the boundary condition for the FE solution in Ω_2. Apply boundary condition at Γ.
4: Copy FE solution obtained at the boundary $\partial\Omega_1$ by solving the problem (3.10) at the Step 2, as the boundary condition for the FE solution in Ω_1.

and the ω-weighted $L^2(\Omega)$ norm

$$\|u\|_\omega := \sqrt{\int_\Omega |u|^2\,\omega d\mathbf{x}}, \qquad \omega > 0, \quad \omega \in L^\infty(\Omega).$$

4.1. Stabilized model

The stabilized formulation for the problem (2.8), with $d = 2, 3$, is now written as:

$$\begin{aligned} s^2\varepsilon(x)\hat{E}(x,s) - \triangle\hat{E}(x,s) - \nabla(\nabla\cdot((\varepsilon-1)\hat{E}(x,s))) &= s\varepsilon(x)f_0(x) \quad x\in\Omega\subset\mathbb{R}^d,\\ \partial_\nu\hat{E}(x,s) &= 0, \quad x\in\Gamma_3,\\ \partial_\nu\hat{E}(x,s) &= f_0(x) - s\hat{E}(x,s), \quad x\in\Gamma_1\cup\Gamma_2, \end{aligned} \tag{4.11}$$

where the second equation in (2.8) is hidden in the first one above.

Below we consider the variational formulation of (4.11) for all $\mathbf{v}\in[H^1(\Omega)]^3$,

$$\begin{aligned} &(s^2\varepsilon\hat{E},\mathbf{v}) + (\nabla\hat{E},\nabla\mathbf{v}) + (\nabla\cdot(\varepsilon\hat{E}),\nabla\cdot\mathbf{v}) - (\nabla\cdot\hat{E},\nabla\cdot\mathbf{v})\\ &- \langle f_0,\mathbf{v}\rangle_{\Gamma_1\cup\Gamma_2} + \langle s\hat{E},\mathbf{v}\rangle_{\Gamma_1\cup\Gamma_2} - \langle\nabla\cdot(\varepsilon\hat{E}) - \nabla\cdot\hat{E},\mathbf{v}\cdot\nu\rangle_\Gamma = (s\varepsilon f_0,\mathbf{v}). \end{aligned} \tag{4.12}$$

Assuming a certain relationship between $|\nabla\varepsilon|$, the lower bound of s: $\underline{s}$, and ε, viz.

$$|\nabla\varepsilon| \le \frac{1}{2}\min(\underline{s}^2\varepsilon, \varepsilon - 1), \tag{4.13}$$

the variational formulation (4.12) for the stabilized problem (4.11) yields an equivalent problem to the original model (2.8).

Assumption 1. By condition (2.5) we may assume that the dielectric permittivity function $\varepsilon(x) \equiv 1$ on a neighborhood of Γ, hence the last boundary integral above is indeed $\equiv 0$. Nevertheless, we have kept this term in order to follow the general path in the computational steps. Fully varying $\varepsilon(x)$, for time dependent problems, is presented in [10,11].

Integration by parts, in the spatial domain, in the second, third and fourth terms in Eq. (4.12) yields; that for all $\mathbf{v}\in[H^1(\Omega)]^3$,

$$\begin{aligned} &(s^2\varepsilon\hat{E},\mathbf{v}) + (\nabla(\nabla\cdot\hat{E}),\mathbf{v}) - (\triangle\hat{E},\mathbf{v}) - (\nabla(\nabla\cdot(\varepsilon\hat{E})),\mathbf{v}) - \langle f_0,\mathbf{v}\rangle_{\Gamma_1\cup\Gamma_2} + \langle s\hat{E},\mathbf{v}\rangle_{\Gamma_1\cup\Gamma_2}\\ &- \langle\nabla\cdot(\varepsilon\hat{E}) - \nabla\cdot\hat{E},\mathbf{v}\cdot\nu\rangle_\Gamma + \langle\partial_\nu\hat{E},\mathbf{v}\rangle_\Gamma + \langle\nabla\cdot(\varepsilon\hat{E}) - \nabla\cdot\hat{E},\mathbf{v}\cdot\nu\rangle_\Gamma = (s\varepsilon f_0,\mathbf{v}), \end{aligned} \tag{4.14}$$

which, canceling the zero terms $\pm\langle\nabla\cdot(\varepsilon\hat{E}) - \nabla\cdot\hat{E},\mathbf{v}\cdot\nu\rangle_\Gamma \equiv 0$, is simplified as

$$\begin{aligned} &(s^2\varepsilon\hat{E},\mathbf{v}) + (\nabla(\nabla\cdot\hat{E}),\mathbf{v}) - (\triangle\hat{E},\mathbf{v}) - (\nabla(\nabla\cdot(\varepsilon\hat{E})),\mathbf{v})\\ &- \langle f_0,\mathbf{v}\rangle_{\Gamma_1\cup\Gamma_2} + \langle s\hat{E},\mathbf{v}\rangle_{\Gamma_1\cup\Gamma_2} + \langle\partial_\nu\hat{E},\mathbf{v}\rangle_{\Gamma_1\cup\Gamma_2} = (s\varepsilon f_0,\mathbf{v}), \quad \forall\mathbf{v}\in[H^1(\Omega)]^3. \end{aligned} \tag{4.15}$$

From this equation, (4.11), and comparing with (2.8), it follows that $\nabla\cdot(\varepsilon\hat{E}) = 0$. To see this, we let $\tilde{E}$ be the unique solution of the problem (2.8) and consider the difference $\bar{E} = \hat{E} - \tilde{E}$ between the solution $\hat{E}$ of the problem (4.11) and the solution $\tilde{E}$ of the problem (2.8). We observe that the function $\bar{E}$ is the solution of the following

homogeneous boundary value problem:

$$\begin{aligned} s^2\varepsilon\bar{E} - \Delta\bar{E} - \nabla(\nabla\cdot((\varepsilon-1)\bar{E})) &= 0 \qquad \text{in } \Omega,\\ \partial_\nu\bar{E} &= -s\bar{E} \qquad \text{on } \Gamma_1\cup\Gamma_2,\\ \partial_\nu\bar{E} &= 0 \qquad \text{on } \Gamma_3. \end{aligned} \tag{4.16}$$

Now we multiply Eq. (4.16) by $\mathbf{v}\in[H^1(\Omega)]^3$ and integrate over Ω to get:

$$(s^2\varepsilon\bar{E},\mathbf{v}) + (\nabla\bar{E},\nabla\mathbf{v}) - (\nabla(\nabla\cdot((\varepsilon-1)\bar{E})),\mathbf{v}) + \langle s\bar{E},\mathbf{v}\rangle_{\Gamma_1\cup\Gamma_2} = 0 \quad \text{in } \Omega. \tag{4.17}$$

Integrating by parts, and using $\varepsilon\equiv 1$ in Ω_2, the third term in (4.17) can be written as

$$\begin{aligned} -(\nabla(\nabla\cdot((\varepsilon-1)\bar{E})),\mathbf{v}) &= \Big(\nabla\cdot((\varepsilon-1)\bar{E}),\nabla\cdot\mathbf{v}\Big) - \langle\nabla(\varepsilon-1)\bar{E},\nu\cdot\mathbf{v}\rangle_\Gamma\\ &- \langle(\varepsilon-1)\nabla\cdot\bar{E},\nu\cdot\mathbf{v}\rangle_\Gamma = \Big((\nabla(\varepsilon-1))\bar{E},\nabla\cdot\mathbf{v}\Big) + \Big((\varepsilon-1)\nabla\cdot\bar{E},\nabla\cdot\mathbf{v}\Big) := I_1+I_2, \end{aligned} \tag{4.18}$$

where the boundary term is vanished because $\varepsilon\equiv 1$ at Γ. Setting $\mathbf{v}=\bar{E}$ in (4.17), and inserting terms corresponding to I_1 and I_2 we end up with

$$\|\bar{E}\|^2_{s^2\varepsilon} + \|\nabla\bar{E}\|^2 + \|\nabla\cdot\bar{E}\|^2_{(\varepsilon-1)} + \|\bar{E}\|^2_{s,\Gamma_1\cup\Gamma_2} + \Big((\nabla(\varepsilon-1))\bar{E},\nabla\cdot\bar{E}\Big) = 0. \tag{4.19}$$

Estimating the last term in (4.19) as the right hand side we have

$$\begin{aligned} -\Big((\nabla(\varepsilon-1))\bar{E},\nabla\cdot\bar{E}\Big) &= -\Big((\nabla\varepsilon)\bar{E},\nabla\cdot\bar{E}\Big)\\ &\le \frac{1}{2}\left\|\bar{E}\right\|^2_{|\nabla\varepsilon|} + \frac{1}{2}\left\|\nabla\cdot\bar{E}\right\|^2_{|\nabla\varepsilon|}. \end{aligned} \tag{4.20}$$

Now, recalling (4.13), we may use (4.19) and (4.20) to get $\bar{E}\equiv 0$ and hence, $\hat{E}=\tilde{E}$, or the solution $\hat{E}$ of the stabilized problem (4.11) is the same as the solution $\tilde{E}$ of the original problem (2.8).

4.2. Finite element discretization

We consider a partition of Ω into elements K denoted by $\mathcal{T}_h=\{K\}$, satisfying the standard finite element subdivision with the minimal angle condition of elements $K\in\mathcal{T}_h$. Here, $h=h(x)$ is a mesh function defined as $h|_K=h_K$, representing the local diameter of the elements, see details in [4]. To formulate the finite element method for (4.11) in Ω, we introduce the, continuous, piecewise linear, finite element space $W_h^E(\Omega)$ for every component of the electric field E defined by

$$W_h^E(\Omega) := \{w\in H^1(\Omega) : w|_K\in P_1(K),\ \ \forall K\in\mathcal{T}_h\},$$

where $P_1(K)$ denote the set of, continuous, piecewise-linear functions on K. Setting $\mathbf{W}_h^E(\Omega) := [W_h^E(\Omega)]^d$, where $d=2,3$. L_2- projection of f_0 with the extra property that it satisfies in the discrete version of the boundary condition in problem (4.11). Then the finite element method for the problem (4.11) in Ω is formulated as:

Find $\hat{E}_h\in\mathbf{W}_h^E(\Omega)$ *such that* $\forall\mathbf{v}\in\mathbf{W}_h^E(\Omega)$

$$\begin{aligned} &(s^2\varepsilon\hat{E}_h,\mathbf{v}) + (\nabla\hat{E}_h,\nabla\mathbf{v}) + (\nabla\cdot(\varepsilon\hat{E}_h),\nabla\cdot\mathbf{v}) - (\nabla\cdot\hat{E}_h,\nabla\cdot\mathbf{v})\\ &+ \langle s\hat{E}_h,\mathbf{v}\rangle_{\Gamma_1\cup\Gamma_2} = (s\varepsilon\mathscr{P}_h f_0,\mathbf{v}) + \langle\mathscr{P}_h f_0,\mathbf{v}\rangle_{\Gamma_1\cup\Gamma_2}. \end{aligned} \tag{4.21}$$

Since $\varepsilon\equiv 1$ on Γ, the outer boundary terms: $\pm\langle\nabla\cdot(\varepsilon\hat{E}) - \nabla\cdot\hat{E},\nu\cdot\mathbf{v}\rangle_\Gamma$ in (4.12) and (4.14) are canceled, and hence do not appear in (4.21) and the subsequent relations.

Theorem 1 (*Well-posedness*)**.** *Under the condition* (4.13) *and with*

$$\mathscr{P}_h f_0\in L_{2,\varepsilon}\cap L_{2,1/s}(\Gamma_1\cup\Gamma_2), \tag{4.22}$$

where $L_{2,\varepsilon}$ *and* $L_{2,1/s}(\Gamma_1\cup\Gamma_2)$ *are the usual* ε*-weighted* $L_2(\Omega)$ *and* $1/s$*-weighted* $L_2(\Gamma_1\cup\Gamma_2)$ *spaces, respectively, the problem* (4.21) *has a unique solution* $\hat{E}_h\in\mathbf{W}_h^E(\Omega)$.

Proof. We define the, discrete, bilinear and linear forms, respectively, as

$$\begin{aligned} a(\hat{E}_h, \mathbf{v}) =& (s^2\varepsilon\hat{E}_h, \mathbf{v}) + (\nabla\hat{E}_h, \nabla\mathbf{v}) + (\nabla\cdot(\varepsilon\hat{E}_h), \nabla\cdot\mathbf{v}) - (\nabla\cdot\hat{E}_h, \nabla\cdot\mathbf{v}) \\ &+ \langle s\hat{E}_h, \mathbf{v}\rangle_{\Gamma_1\cup\Gamma_2}, \end{aligned} \tag{4.23}$$

and

$$\mathscr{L}(\mathbf{v}) \coloneqq (s\varepsilon\mathscr{P}_h f_0, \mathbf{v}) + \langle\mathscr{P}_h f_0, \mathbf{v}\rangle_{\Gamma_1\cup\Gamma_2},$$

and restate Eq. (4.21) in its compact form as

$$a(\hat{E}_h, \mathbf{v}) = \mathscr{L}(\mathbf{v}). \tag{4.24}$$

Thus, for the well-posedness via a Lax–Milgram like approach, it suffices to show that the discrete bilinear form $a(\cdot,\cdot)$ is coercive, and both $a(\cdot,\cdot)$ and $\mathscr{L}(\cdot)$ are continuous. To this end we introduce the triple norm

$$|||\hat{E}_h|||^2 \coloneqq \| \hat{E}_h \|^2_{s^2\varepsilon} + \| \nabla\hat{E}_h \|^2 + \| \nabla\cdot\hat{E}_h \|^2_{\varepsilon^{-1}} + \| \hat{E}_h \|^2_{s,\Gamma_1\cup\Gamma_2}. \tag{4.25}$$

The proof of theorem is now a result of the following well-posedness inequalities: There are constants $C_i,\ i = 2, 3$ such that for all $\hat{E}_h$ and $\mathbf{v} \in \mathbf{W}_h^E(\Omega)$,

$$a(\hat{E}_h, \hat{E}_h) \geq \frac{1}{2}|||\hat{E}_h|||^2 \qquad \text{(Coercivity of } a\text{)}, \tag{4.26}$$

$$a(\hat{E}_h, \mathbf{v}) \leq C_2|||\hat{E}_h||| \cdot |||\mathbf{v}|||, \qquad \text{(Continuity of } a\text{)}, \tag{4.27}$$

$$|\mathscr{L}(\mathbf{v})| \leq C_3|||\mathbf{v}|||, \qquad \text{(Continuity of } \mathscr{L}\text{)}. \tag{4.28}$$

Here, to justify the well-posedness, we do not need the, additional, stabilization bilinear form as in [3], [45], and rely on the approach by, e.g. [16,17], and [33], that yields discrete coercivity, and hence also discrete stability.

To derive (4.26) is straightforward: letting $\mathbf{v} = \hat{E}_h$ in (4.23),

$$\begin{aligned} a(\hat{E}_h, \hat{E}_h) &= (s^2\varepsilon\hat{E}_h, \hat{E}_h) + (\nabla\hat{E}_h, \nabla\hat{E}_h) + (\nabla(\varepsilon-1)\hat{E}_h, \nabla\cdot\hat{E}_h) \\ &+ ((\varepsilon-1)\nabla\cdot\hat{E}_h, \nabla\cdot\hat{E}_h) + \langle s\hat{E}_h, \hat{E}_h\rangle_{\Gamma_1\cup\Gamma_2} \\ &= \| \hat{E}_h \|^2_{s^2\varepsilon} + \| \nabla\hat{E}_h \|^2 + \| \nabla\cdot\hat{E}_h \|^2_{\varepsilon^{-1}} \\ &+ (\nabla(\varepsilon-1)\hat{E}_h, \nabla\cdot\hat{E}_h) + \| \hat{E}_h \|^2_{s,\Gamma_1\cup\Gamma_2}. \end{aligned} \tag{4.29}$$

where we have used the equality

$$\begin{aligned} (\nabla\cdot(\varepsilon\hat{E}_h), \nabla\cdot\mathbf{v}) - (\nabla\cdot\hat{E}_h, \nabla\cdot\mathbf{v}) &= (\nabla\cdot((\varepsilon-1)\hat{E}_h), \nabla\cdot\mathbf{v}) \\ &= (\nabla(\varepsilon-1)\hat{E}_h + (\varepsilon-1)\nabla\cdot\hat{E}_h, \nabla\cdot\mathbf{v}). \end{aligned} \tag{4.30}$$

Here, using $\nabla(\varepsilon-1) = \nabla\varepsilon$, the contribution from the first term on the right hand side can be estimated, from above, as

$$\pm\Big((\nabla\varepsilon)\hat{E}_h, \nabla\cdot\hat{E}_h\Big) \geq -\frac{1}{2}\left\|\hat{E}_h\right\|^2_{|\nabla\varepsilon|} - \frac{1}{2}\left\|\nabla\cdot\hat{E}_h\right\|^2_{|\nabla\varepsilon|}, \tag{4.31}$$

which recalling the assumption (4.13), can be hidden in the first and third terms in the triple norm and proves the coercivity.

As for the continuity of $a(\cdot,\cdot)$, using *Cauchy–Schwarz' inequality* and (4.31),

$$\begin{aligned} a(\hat{E}_h, \mathbf{v}) &= (s^2\varepsilon\hat{E}_h, \mathbf{v}) + (\nabla\hat{E}_h, \nabla\mathbf{v}) + (\nabla\cdot((\varepsilon-1)\hat{E}_h), \nabla\cdot\mathbf{v}) + \langle s\hat{E}_h, \mathbf{v}\rangle_{\Gamma_1\cup\Gamma_2} \\ &= (s\sqrt{\varepsilon}\hat{E}_h, s\sqrt{\varepsilon}\mathbf{v}) + (\nabla\hat{E}_h, \nabla\mathbf{v}) + ((\varepsilon-1)\nabla\cdot\hat{E}_h, \nabla\cdot\mathbf{v}) \\ &+ ((\nabla\varepsilon)\hat{E}_h, \nabla\cdot\mathbf{v}) + \langle\sqrt{s}\hat{E}_h, \sqrt{s}\mathbf{v}\rangle_{\Gamma_1\cup\Gamma_2} \\ &\leq \| \hat{E}_h \|_{s^2\varepsilon}\| \mathbf{v} \|_{s^2\varepsilon} + \| \nabla\hat{E}_h \|\| \nabla\mathbf{v} \| + \| \nabla\cdot\hat{E}_h \|_{\varepsilon^{-1}}\| \nabla\cdot\mathbf{v} \|_{\varepsilon^{-1}} \\ &+ \| \hat{E}_h \|_{|\nabla\varepsilon|}\| \nabla\cdot\mathbf{v} \|_{|\nabla\varepsilon|} + \| \hat{E}_h \|_{s,\Gamma_1\cup\Gamma_2}\| \mathbf{v} \|_{s,\Gamma_1\cup\Gamma_2} \\ &\leq C|||\hat{E}_h||| \cdot |||\mathbf{v}|||, \qquad \forall\mathbf{v} \in \mathbf{W}_h^E(\Omega). \end{aligned} \tag{4.32}$$

Likewise, for $\mathscr{P}_h f_{0,h} \in L_{2,\varepsilon}(\Omega) \cap L_{2,1/s}(\Gamma_1 \cup \Gamma_2)$, we can easily verify that

$$\begin{aligned}\mathscr{L}(\mathbf{v}) &= \left(\sqrt{\varepsilon}\mathscr{P}_h f_0, s\sqrt{\varepsilon}\mathbf{v}\right) + \langle \mathscr{P}_h f_0, \mathbf{v}\rangle_{\Gamma_1\cup\Gamma_2} \\ &\le \| \mathscr{P}_h f_0 \|_\varepsilon \| \mathbf{v} \|_{s^2\varepsilon} + \| \mathscr{P}_h f_0 \|_{1/s,\Gamma_1\cup\Gamma_2} \| \mathbf{v} \|_{s,\Gamma_1\cup\Gamma_2} \\ &\le \left(\| \mathscr{P}_h f_0 \|_\varepsilon + \| \mathscr{P}_h f_0 \|_{1/s,\Gamma_1\cup\Gamma_2}\right) |||\mathbf{v}|||,\end{aligned} \tag{4.33}$$

and hence $\mathscr{L}$ is continuous as well, and the proof is complete.

5. Error analysis

In this section first we prove an *a priori error bound* based on an additional assumption on ε, and then continue with a posteriori error estimates for the continuous piecewise linear approximation of time harmonic Maxwell's equations formulated in (4.21).

5.1. A priori error estimates

To derive a priori error estimates we need the continuous versions of the linear and bilinear forms introduced in the well-posedness theorem. To this end, we rewrite (4.23) replacing $\hat{E}_h$ by $\hat{E}$ and with a new continuous linear form defined with the same expression as $\mathscr{L}(\mathbf{v})$, but for $\mathbf{v} \in [H^1(\Omega)]^d$ rather than in the space $\mathbf{W}_h^E(\Omega)$:

$$\begin{aligned}a(\hat{E}, \mathbf{v}) =&(s^2\varepsilon\hat{E}, \mathbf{v}) + (\nabla\hat{E}, \nabla\mathbf{v}) + (\nabla\cdot(\varepsilon\hat{E}), \nabla\cdot\mathbf{v}) \\ &- (\nabla\cdot\hat{E}, \nabla\cdot\mathbf{v}) + \langle s\hat{E}, \mathbf{v}\rangle_{\Gamma_1\cup\Gamma_2}, \qquad \forall\mathbf{v} \in [H^1(\Omega)]^d\end{aligned} \tag{5.34}$$

and

$$\mathscr{L}^c(\mathbf{v}) := (s\varepsilon f_0, \mathbf{v}) + \langle f_0, \mathbf{v}\rangle_{\Gamma_1\cup\Gamma_2}, \qquad \forall\mathbf{v} \in [H^1(\Omega)]^d. \tag{5.35}$$

Hence we have the concise form of the variational formulation

$$a(\hat{E}, \mathbf{v}) = \mathscr{L}^c(\mathbf{v}), \qquad \forall\mathbf{v} \in [H^1(\Omega)]^d. \tag{5.36}$$

To proceed we derive a *quasi Galerkin orthogonality* relation by restricting, in (5.34) and (5.35), $\mathbf{v} \in \mathbf{W}_h^E(\Omega)$, and then subtracting (4.24) from the, such obtained, version of the continuous problem (5.36) to get

$$\begin{aligned}a(\hat{E} - \hat{E}_h, \mathbf{v}) &= \mathscr{L}^c(\mathbf{v}) - \mathscr{L}(\mathbf{v}) \\ &= \left(s\varepsilon(f_0 - \mathscr{P}_h f_0), \mathbf{v}\right) + \langle f_0 - \mathscr{P}_h f_0, \mathbf{v}\rangle_{\Gamma_1\cup\Gamma_2}, \quad \forall\mathbf{v} \in \mathbf{W}_h^E(\Omega).\end{aligned} \tag{5.37}$$

For the P1 approximation, using the linear interpolant $\mathscr{P}_h f_0$ of $f_0 \in L^2(\Omega)$, we may assume that, the weighted difference $\|f_0 - \mathscr{P}_h f_0\|_\varepsilon$ is of the order $\mathscr{O}(h)$:

$$\|f_0 - \mathscr{P}_h f_0\|_\varepsilon \sim |f_0 - \mathscr{P}_h f_0|_{1/s,\Gamma_1\cup\Gamma_2} (\sim \mathscr{O}(h)). \tag{5.38}$$

Usually, we need more than $f_0 \in L^2(\Omega)$ to have the $O(h)$ estimate which we assumed is the case for f_0 here. The relation in (5.38) is straightforward in non-weighted norms.

Now we are ready to derive the following theoretical error bound.

Theorem 2. *Let $\hat{E}$ and $\hat{E}_h$ be the solutions for the continuous problem (4.11) (in the variational form (4.12)) and its finite element approximation, (4.21), respectively. Then, assuming (5.38), as well as adequate lower bounds for the coefficients $s^2\varepsilon$ and $(\varepsilon - 1)$ there is a constant C, independent of $\hat{E}$ and h, such that*

$$|||e||| \le C \| h\hat{E} \|_{H^2_w(\Omega)} + \mathscr{O}(h).$$

where $w = w(\varepsilon(x), s)$ is the weight function which depends on the dielectric permittivity function $\varepsilon(x)$ and the pseudo-frequency variable s. Further, $\mathscr{O}(h)$, corresponds to the contributions from the interpolation and L_2-projection errors in (5.38).

Proof. Let $e = \hat{E} - \hat{E}_h$, using the quasi Galerkin orthogonality (5.37), applied to the term $a(e, \hat{E}_h)$ below, we have that

$$\begin{aligned} a(e,e) &= a(e, \hat{E} - \hat{E}_h) = a(e, \hat{E}) - a(e, \hat{E}_h) \\ &= a(e, \hat{E}) - \left(s\varepsilon(f_0 - \mathscr{P}_h f_0), \hat{E}_h\right) - \langle f_0 - \mathscr{P}_h f_0, \hat{E}_h\rangle_{\Gamma_1\cup\Gamma_2} \\ &= a(e, \hat{E} - \pi_h\hat{E}) + a(e, \pi_h\hat{E}) - \left(s\varepsilon(f_0 - \mathscr{P}_h f_0), \hat{E}_h\right) \\ &\quad - \langle f_0 - \mathscr{P}_h f_0, \hat{E}_h\rangle_{\Gamma_1\cup\Gamma_2}. \end{aligned} \tag{5.39}$$

Next, we apply the quasi Galerkin orthogonality (5.37) to term $a(e, \pi_h\hat{E})$ above, and combine the initial data terms appearing on the right hand side to get

$$\begin{aligned} a(e,e) =& a(e, \hat{E} - \pi_h\hat{E}) \\ &+ \left(s\varepsilon(f_0 - \mathscr{P}_h f_0), \pi_h\hat{E} - \hat{E}_h\right) + \langle f_0 - \mathscr{P}_h f_0, \pi_h\hat{E} - \hat{E}_h\rangle_{\Gamma_1\cup\Gamma_2}. \end{aligned} \tag{5.40}$$

Now using the Cauchy–Schwarz' inequality and the interpolation error estimates we can estimate the first term on the right hand side of (5.40) as follows:

$$\begin{aligned} a(e, \hat{E} - \pi_h\hat{E}) &= (e, \hat{E} - \pi_h\hat{E})_{s^2\varepsilon} + (\nabla e, \nabla(\hat{E} - \pi_h\hat{E})) + (\nabla\cdot e, \nabla\cdot(\hat{E} - \pi_h\hat{E}))_{\varepsilon-1} \\ &\quad + ((\nabla\varepsilon)e, \nabla(\hat{E} - \pi_h\hat{E})) \\ &\le \| e \|_{s^2\varepsilon}\| \hat{E} - \pi_h\hat{E} \|_{s^2\varepsilon} + \| \nabla e \|\| \nabla(\hat{E} - \pi_h\hat{E}) \| \\ &\quad + \| \nabla\cdot e \|_{\varepsilon-1}\| \nabla\cdot(\hat{E} - \pi_h\hat{E}) \|_{\varepsilon-1} + \| e \|_{|\nabla\varepsilon|}\| \nabla\cdot(\hat{E} - \pi_h\hat{E}) \|_{|\nabla\varepsilon|} \\ &\quad + \| e \|_{s,\Gamma_1\cup\Gamma_2}\| \hat{E} - \pi_h\hat{E} \|_{s,\Gamma_1\cup\Gamma_2} \\ &\le c_1 \| e \|_{s^2\varepsilon}\| h^2D^2\hat{E} \|_{s^2\varepsilon} + c_2 \| \nabla e \|\| hD^2\hat{E} \| + \\ &\quad + c_2 \| \nabla\cdot e \|_{\varepsilon-1}\| hD^2\hat{E} \|_{\varepsilon-1} + c_2 \| e \|_{|\nabla\varepsilon|}\| hD^2\hat{E} \|_{|\nabla\varepsilon|} \\ &\quad + c_4 \| e \|_{s,\Gamma_1\cup\Gamma_2} \left(\| h^2D^2\hat{E} \|^{1/2}_{s,L_2(\Omega)} \cdot \| hD^2\hat{E} \|^{1/2}_{s,L_2(\Omega)}\right). \end{aligned}$$

Thus, we have

$$\begin{aligned} a(e, \hat{E} - \pi_h\hat{E}) \le& C|||e||| \cdot \left(\| h^2D^2\hat{E} \|_{s^2\varepsilon} + \| hD^2\hat{E} \| + \| hD^2\hat{E} \|_{\varepsilon-1}\right) \\ &+ \| hD^2\hat{E} \|_{|\nabla\varepsilon|} + \| h^{3/2}D^2\hat{E} \|_s \le C|||e|||\cdot \| hD^2\hat{E} \|_w \end{aligned} \tag{5.41}$$

where we used (4.13), $w = \max(hs^2\varepsilon, \varepsilon - 1, h^{1/2}s)$, and to estimate the interpolation error at the boundary we applied the trace estimate (see Brenner–Scott [15]).

$$\begin{aligned} \| \hat{E} - \pi_h\hat{E} \|_{s,\Gamma} &\le \tilde{C} \| \hat{E} - \pi_h\hat{E} \|^{1/2}_{s,L_2(\Omega)}\| \hat{E} - \pi_h\hat{E} \|^{1/2}_{s,H^1(\Omega)} \\ &\le \tilde{C} \| \hat{E} - \pi_h\hat{E} \|^{1/2}_{s,L_2(\Omega)}\| \nabla(\hat{E} - \pi_h\hat{E}) \|^{1/2}_{s,L_2(\Omega)} \\ &\le \tilde{C} \| h^2D^2\hat{E} \|^{1/2}_{s,L_2(\Omega)} \cdot \| hD^2\hat{E} \|^{1/2}_{s,L_2(\Omega)} . \end{aligned} \tag{5.42}$$

Here, D^2 stands for the differential operator which, e.g. for the 2-dimensional domain Ω, i.e. in xy-geometry and for $u \in \mathscr{C}^{(2)}(\Omega)$ is given by

$$D^2u := (u^2_{xx} + 2u^2_{xy} + u^2_{yy})^{1/2}.$$

Finally, $\tilde{C}$ is a general constant and c_i:s are the interpolation constants. Hence, recalling the definition (4.25) of the triple norm, coercivity and continuity of $a(e,e)$ (see (4.26) and (4.27)) which also hold for functions in $H^1(\Omega)$, assumptions (5.38) on the order of interpolation and L_2-projection errors, a kick-back argument yields the result.

Remark 3. We note that the obtained error is of order $\mathcal{O}(h)$ in $H^2_w(\Omega)$ which is optimal due to the gradient term in the triple norm. This may be further improved to achieve superconvergence and estimations in the negative norm which in scalar form is defined as

$$\|w\|_{H^{-s}(\Omega)} = \sup_{\varphi\in H^s(\Omega)\cap H^1_0(\Omega)} \frac{(w,\varphi)}{\|\varphi\|_{H^s(\Omega)}}.$$

This, however, extended to vector form, yields extra computational complexity. Besides in P_1 approximation the contributions from the assumption on interpolation error of the initial data deteriorates any convergence rate beyond $\mathcal{O}(h)$.

5.2. A posteriori error estimates

In the *a posteriori* error estimates we need the residual (loosely speaking, the difference between the left and the right hand side of the continuous equation, when the exact solution is replaced by its current approximation). Starting from the finite element formulation, the residual is obtained through the converse use of Green's formula, resulting inter-element jump terms at the element-boundaries. In the discrete formulations, the second order derivatives are defined as in the form of discrete Laplacian:

$$\begin{aligned}(\Delta_h \mathbf{u}_h, \mathbf{v}_h) &:= -(\nabla \mathbf{u}_h, \nabla \mathbf{v}_h) + \sum_{K\in\mathcal{T}_h}\int_{\partial K} [\nabla \mathbf{u}_h \cdot \nu]\, \mathbf{v}_h \, d\sigma,\\ (\nabla \mathbf{u}_h, \nabla \mathbf{v}_h) &:= \sum_{K\in\mathcal{T}_h}\int_K \nabla \mathbf{u}_h \cdot \nabla \mathbf{v}_h d\mathbf{x}, \quad \forall \mathbf{u}_h\ ,\ \mathbf{v}_h \in \mathbf{W}^E_h(\Omega).\end{aligned} \tag{5.43}$$

Now if we relabel the boundaries of the internal element as

$$\partial K_\pm = \{\sigma \in \partial K : \xi(\sigma)\cdot\nu(\sigma) \geq (<)0\}, \quad \xi = \nabla \mathbf{u}, \ \text{ or } \ \xi = \nabla \mathbf{u}_h,$$

then the jump is:

$$[\xi\cdot\nu]\Big|_{\partial K} = \xi\cdot\nu\Big|_{\partial K_+} - \xi\cdot\nu\Big|_{\partial K_-}.$$

If K_1 and K_2 are two elements with a common side S, and $\xi = \nabla \mathbf{u}$, then $\partial K_{1,+}\Big|_S = \partial K_{2,-}\Big|_S$ and hence the whole contributions from the jumps will cancel out except the integrals over the outer boundaries where there are no jumps, (see, e.g. [38], p. 193). Note that in the elliptic type problems, the natural boundary condition is (see, e.g. [15] p142):

$$\sum_{\partial K\in\partial\mathcal{T}_h}\int_{\partial K} [\nabla \mathbf{u}\cdot\nu]\, \mathbf{v}_h \, d\sigma = 0. \tag{5.44}$$

However, the contribution of discrete jumps are non-zero:

$$\sum_{\partial K\in\partial\mathcal{T}_h}\int_{\partial K} [\nabla \mathbf{u}_h\cdot\nu]\, \mathbf{v}_h \, d\sigma \neq 0, \tag{5.45}$$

and therefore are involved in the weak formulations. Here, $\partial\mathcal{T}_h = \{\partial K\}$: is the set of all boundaries ∂K of elements $K \in \mathcal{T}_h$, and we denote by $\mathcal{S}_\Gamma \subset \partial\mathcal{T}_h$, the set of all sides ∂K of the elements K such that 2 or 3 vertices of these elements, a side in 2- and a surface in 3-dimensions, respectively, belongs to Γ.

We also introduce the local measuring environments (scalar product and norm):

$$(u,v)_K := \int_K u\cdot v \ d\mathbf{x}, \quad (u,v)_K := \int_K u\cdot v\ \omega d\mathbf{x}, \quad \langle u,v\rangle_\Gamma := \int_{\partial K} u\cdot v\ d\sigma,$$

and local ω-weighted $L^2(K)$-norm

$$\|u\|_{K,\omega} := \sqrt{\int_K |u|^2\,\omega d\mathbf{x}}, \qquad \omega > 0, \quad \omega \in L^\infty(K).$$

Then, the global scalar product and norm are the obvious sums,

$$(u,v)_\Omega = \sum_{K\in\mathcal{T}_h}(u,v)_K, \qquad \|u\|_\Omega^2 = \sum_{K\in\mathcal{T}_h}\|u\|_K^2 .$$

We may define the residuals as

$$\begin{aligned}
-\mathscr{R}(\hat{E}_h) :=& s^2\varepsilon(x)\hat{E}_h - \Delta_h\hat{E}_h - \nabla_h(\nabla\cdot((\varepsilon(x)-1)\hat{E}_h)) - s\varepsilon(x)f_0(x), \quad \text{or}\\
-\mathscr{R}_h(\hat{E}_h) :=& s^2\varepsilon(x)\hat{E}_h - \Delta_h\hat{E}_h, e)_K + \sum_{K\in\mathcal{T}_h}(\nabla_h(\nabla\cdot((\varepsilon(x)-1)\hat{E}_h), e))_K\\
&- \sum_{\partial K\in\partial\mathcal{T}_h}\frac{1}{2}\int_{\partial K}\Big[\Big(\nabla\hat{E}_h + \nabla\cdot((\varepsilon-1)\hat{E}_h)\Big)\cdot\nu\Big]e\,d\sigma - \langle s\hat{E}_h, e\rangle_{\Gamma_1\cup\Gamma_2}.
\end{aligned} \tag{5.46}$$

Thus using the notation for $\mathscr{R}_h(\hat{E}_h)$, and $\eta = (\nabla\hat{E}_h + \nabla\cdot((\varepsilon-1)\hat{E}_h))\cdot\nu$ on $\partial K\in\partial\mathcal{T}_h$, we write the above equation (interpreting the scalar products involving twice differentiation as sums and noting that $\langle\partial_\nu\hat{E}_h + s\hat{E}_h, e\rangle_{\Gamma_1\cup\Gamma_2} = \langle\mathscr{P}_h f_0, e\rangle_{\Gamma_1\cup\Gamma_2}$ as

$$\begin{aligned}
a(e,e) =& (s\varepsilon(f_0-\mathscr{P}_h f_0), e) + (\mathscr{R}_E(\hat{E}_h), e) + \langle(f_0-\mathscr{P}_h f_0), e\rangle_{\Gamma_1\cup\Gamma_2}\\
&+ \langle\partial_\nu\hat{E}_h + s\hat{E}_h, e\rangle_{\Gamma_1\cup\Gamma_2} - \frac{1}{2}\sum_{\partial K\in\partial\mathcal{T}_h}\langle[\eta], e\rangle_{\partial K} - \langle s\hat{E}_h, e\rangle_{\Gamma_1\cup\Gamma_2}\\
=& (s\varepsilon(f_0-\mathscr{P}_h f_0), e) + (\mathscr{R}_E(\hat{E}_h), e) + \langle f_0-\mathscr{P}_h f_0, e\rangle_{\Gamma_1\cup\Gamma_2}\\
&+ \langle\partial_\nu\hat{E}_h, e\rangle_{\Gamma_1\cup\Gamma_2} - \frac{1}{2}\sum_{\partial K\in\partial\mathcal{T}_h}\langle[\eta], e\rangle_{\partial K},
\end{aligned} \tag{5.47}$$

where, in above the $\pm\langle s\hat{E}_h, e\rangle_{\Gamma_1\cup\Gamma_2}$ terms are canceled. With the presence of the L_2 projection $\mathscr{P}_h f_0$, and in view of (5.40) Eq. (5.47) can be rewritten as

$$\begin{aligned}
a(e,e) =& (s\varepsilon(f_0-\mathscr{P}_h f_0), e) + (\mathscr{R}_h(\hat{E}_h), e-\pi_h e) + \langle f_0-\mathscr{P}_h f_0, e\rangle_{\Gamma_1\cup\Gamma_2}\\
&+ \langle\partial_\nu\hat{E}_h, e-\pi_h e\rangle_{\Gamma_1\cup\Gamma_2} - \frac{1}{2}\sum_{\partial K\in\partial\mathcal{T}_h}\langle[\eta], e-\pi_h e\rangle_{\partial K}\\
=& (\sqrt{\varepsilon}(f_0-\mathscr{P}_h f_0), s\sqrt{\varepsilon}e) + (h\mathscr{R}_h(\hat{E}_h), h^{-1}(e-\pi_h e))\\
&+ \langle 1/\sqrt{s}(f_0-\mathscr{P}_h f_0), \sqrt{s}e\rangle_{\Gamma_1\cup\Gamma_2}\\
&+ \sum_{\partial K\in\mathscr{S}_\Gamma}\langle\partial_\nu\hat{E}_h, e-\pi_h e\rangle_{\partial K} - \frac{1}{2}\sum_{\partial K\in\partial\mathcal{T}_h}\langle h_K^{-1}[\eta], (e-\pi_h e)h_K\rangle_{\partial K}\\
\le& \|f_0-\mathscr{P}_h f_0\|_\varepsilon\,\|e\|_{s^2\varepsilon} + C_i\left\|h\mathscr{R}_h(\hat{E}_h)\right\|\,\|\nabla e\| + |f_0-\mathscr{P}_h f_0|_{1/s,\Gamma_1\cup\Gamma_2}\,\|e\|_{s,\Gamma_1\cup\Gamma_2}\\
&+ \max_{\partial K\in\mathscr{S}_\Gamma}\left|h_K^{-1}\partial_\nu\hat{E}_h\right|(h\,\|\nabla e\|) + C_i\frac{1}{2}\max_{\partial K\in\partial\mathcal{T}_h}\{h_K^{-1}\,|[\eta]|\}(h\,\|\nabla e\|)\\
\le& C_i\left\|h\tilde{\mathscr{R}}_h(\hat{E}_h)\right\|\,\|\nabla e\| + Ch\Big(\|e\|_{s^2\varepsilon} + \|e\|_{s,\Gamma_1\cup\Gamma_2}\Big)\\
\le& \tilde{C}_i\Big(h + \left\|h\tilde{\mathscr{R}}_h(\hat{E}_h)\right\|\Big)|||e|||,
\end{aligned}$$

where for the justification for the maximum terms above we refer to [15,30]. Now, recalling the definition of the triple norm and coercivity the proof is complete.

6. Numerical examples

Computations in this section are inspired by the works [10,11], devoted to the study of stabilized time-dependent Maxwell's system. In [10,11], we perform numerical tests in the computational domain $\Omega = [0,1]\times[0,1]$ with $\Omega_1 = [0.25,0.75]\times[0.25,0.75]$. The time dependent model problem with source data $f(\mathbf{x},t)$, $\mathbf{x} := (x,y)\in\mathbb{R}^2$, $t\in$

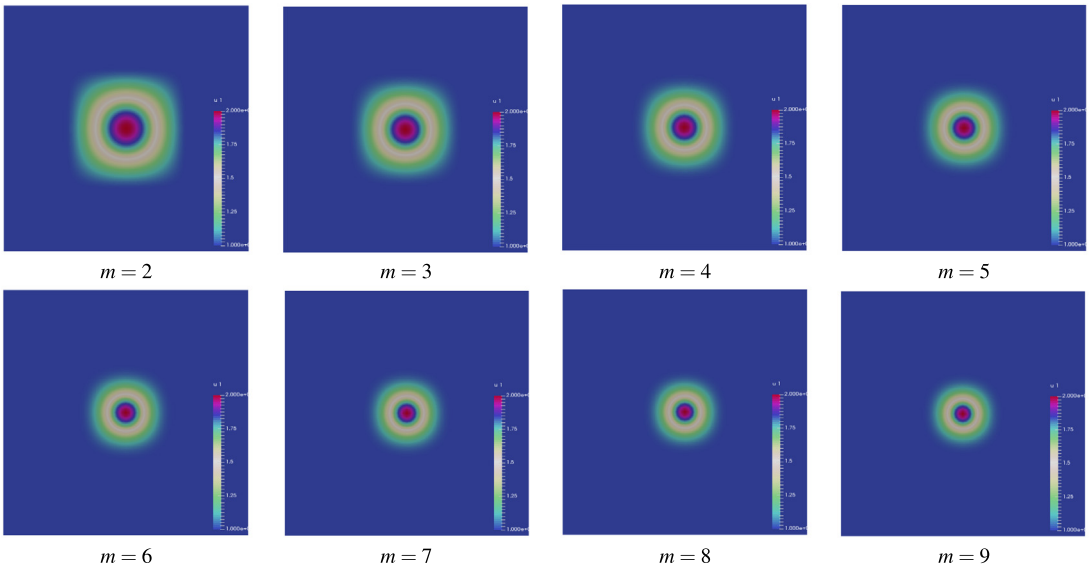

Fig. 2. The function $\varepsilon(x, y)$ in the domain $\Omega = [0, 1] \times [0, 1]$ for different m in (6.51).

$[0, 0.5]$ (the right hand side) is given by:

$$\begin{aligned} \varepsilon(\mathbf{x})\frac{\partial^2 E(\mathbf{x}, t)}{\partial t^2} + \nabla \times \nabla \times E(\mathbf{x}, t) &= f(\mathbf{x}, t), \\ \nabla \cdot (\varepsilon E)(\mathbf{x}, t) &= 0, \\ E(\mathbf{x}, 0) = 0, \quad \frac{\partial E}{\partial t}(\mathbf{x}, 0) &= 0, \\ E|_{\Gamma} &= 0. \end{aligned} \tag{6.48}$$

The electric field $E(\mathbf{x}, t) = (E_1(\mathbf{x}, t), E_2(\mathbf{x}, t))$ is chosen such that the functions

$$\begin{aligned} E_1(\mathbf{x}, t) &= \frac{t^2}{\varepsilon}\pi \sin^2 \pi x \cos \pi y \sin \pi y, \\ E_2(\mathbf{x}, t) &= -\frac{t^2}{\varepsilon}\pi \sin^2 \pi y \cos \pi x \sin \pi x \end{aligned} \tag{6.49}$$

give rise to the exact solution of this problem. After application of the Laplace transform (2.3) to (6.49) the exact solution of the transformed (time harmonic) model problem will be

$$\begin{aligned} \hat{E}_1(\mathbf{x}, s) &= \frac{2}{s^3\varepsilon}\pi \sin^2 \pi x \cos \pi y \sin \pi y, \\ \hat{E}_2(\mathbf{x}, s) &= -\frac{2}{s^3\varepsilon}\pi \sin^2 \pi y \cos \pi x \sin \pi x. \end{aligned} \tag{6.50}$$

In (6.49) the function ε is defined for an integer $m > 1$ as

$$\varepsilon(x, y) = \begin{cases} 1 + \sin^m \pi(2x - 0.5) \cdot \sin^m \pi(2y - 0.5) & \text{in } \Omega_1, \\ 1 & \text{otherwise}, \end{cases} \tag{6.51}$$

such that the condition $\nabla \cdot (\varepsilon E)(x, t) = 0$ is fulfilled. Fig. 2 shows the function ε for different values of $m = 2, \ldots, 9$ which we used in computations.

For numerical solution of (6.48) the software package WavES implemented in C++/PETSc [1] is used [2].

In the time harmonic version, we discretize the computational domain Ω denoting by $\mathcal{T}_{hl} := \{K\}$ a partition of the domain Ω into triangles K of sizes $h_l = 2^{-l}, l = 1, \ldots, 6$. Numerical tests are performed for $s = 20$ in (2.3) (this value is justified by experimental studies in [12,48,49]) and for different $m = 2, \ldots, 9$ in (6.51). The relative

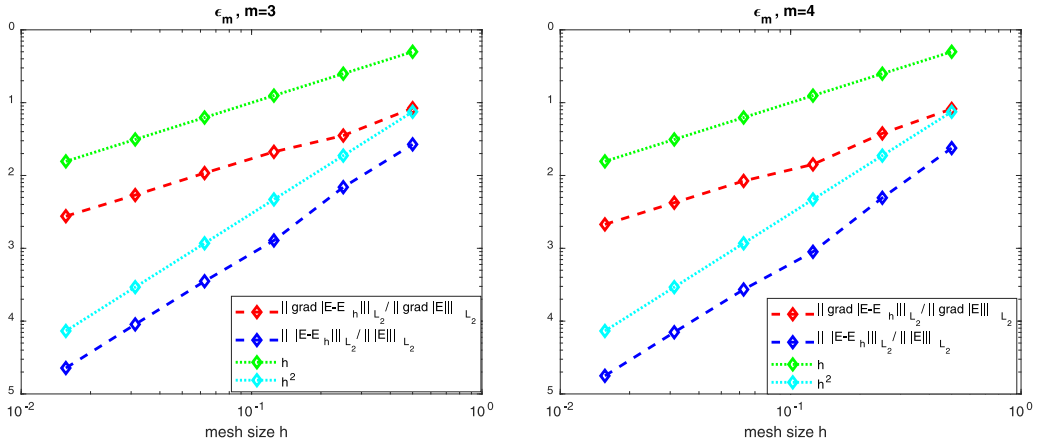

Fig. 3. Relative errors for $m = 3$ (left) and $m = 4$ (right).

errors are then measured in both L_2- and H^1-norms, which are computed as

$$e_l^1 = \frac{\|\hat{E} - \hat{E}_h\|_{L_2}}{\|\hat{E}\|_{L_2}}, \qquad \text{and} \tag{6.52}$$

$$e_l^2 = \frac{\|\nabla(\hat{E} - \hat{E}_h)\|_{L_2}}{\|\nabla\hat{E}\|_{L_2}}, \tag{6.53}$$

respectively, where, as in the sequel

$$\left|\hat{E}\right| := \sqrt{\hat{E}_1^2 + \hat{E}_2^2} \qquad \left|\hat{E}_h\right| := \sqrt{\hat{E}_{1h}^2 + \hat{E}_{2h}^2}. \tag{6.54}$$

Here, $\hat{E} = (\hat{E}_1, \hat{E}_2)$ is the exact solution given by (6.50), and $\hat{E}_h = (\hat{E}_{1h}, \hat{E}_{2h})$ is the computed solution.

Figs. 3–5 present convergence of P1 finite element numerical scheme for the function ε defined by (6.51) and for $m = 3, \ldots, 8$. Convergence rates q_1 and q_2 in these figures are computed according to the logarithmic expressions:

$$\begin{aligned} q_1 &= \frac{\left|\log\left(\frac{el_h^1}{el_{2h}^1}\right)\right|}{|\log(0.5)|}, \\ q_2 &= \frac{\left|\log\left(\frac{el_h^2}{el_{2h}^2}\right)\right|}{|\log(0.5)|}, \end{aligned} \tag{6.55}$$

where el_h^j, el_{2h}^j, $j = 1, 2$ are computed relative norms el^j, $j = 1, 2$ on the mesh $\mathcal{T}_h$ with the mesh size h and $2h$, respectively. Similar convergence rates are obtained for $m = 2, 3, 4, 6, 8, 9$ (these rates are not presented here), see their convergence results in the extended preprint version of this paper [5] and in the short version of the current paper [6].

Figs. 6 show computed $|\hat{E}_h|$ and exact $|\hat{E}|$ solutions on meshes $\mathcal{T}_{hl}$ with the mesh sizes $h_l = 2^{-l}, l = 3, 4, 5, 6$, for $m = 5$ and $m = 7$ in (6.51), respectively.

We have implemented the domain decomposition algorithm as well, see Algorithm 1 of Section 3, taking $\Omega = [0, 1] \times [0, 1]$ and $\Omega_1 := [0.25, 0.75] \times [0.25, 0.75]$ such that $\Omega = \Omega_1 \cup \Omega_2$. Fig. 1 illustrates a such type of domain decomposition for $h = 0.0625$. But since convergence results in the domain decomposition method are similar to the finite element computations in the whole domain Ω, we omit presenting them here. Fig. 7 illustrates computational solution of the problem (6.48) using the domain decomposition method presented in Section 3.

Using Figs. 3–5 we observe that our scheme behaves like a first order method for $H^1(\Omega)$-norm and second order method for $L_2(\Omega)$-norm for all values of m. The obtained numerical results confirm the analytic estimates derived in Theorem 2.

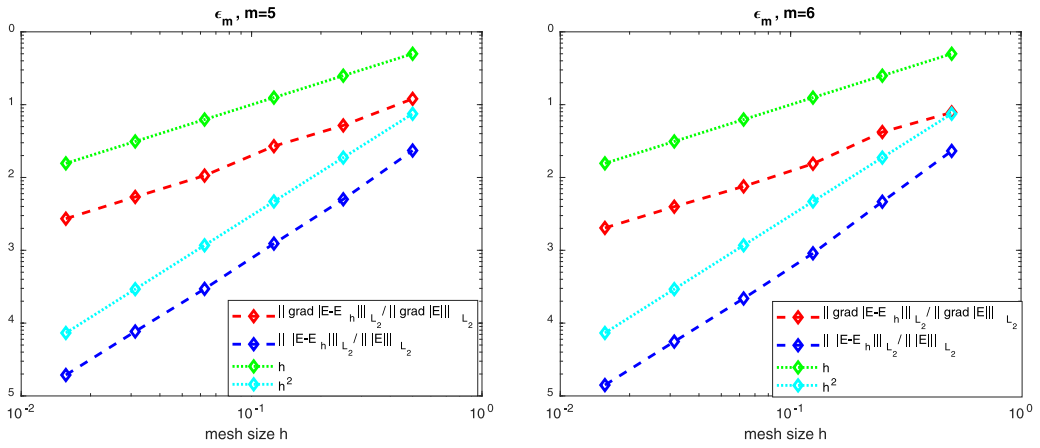

Fig. 4. Relative errors for $m = 5$ (left) and $m = 6$ (right).

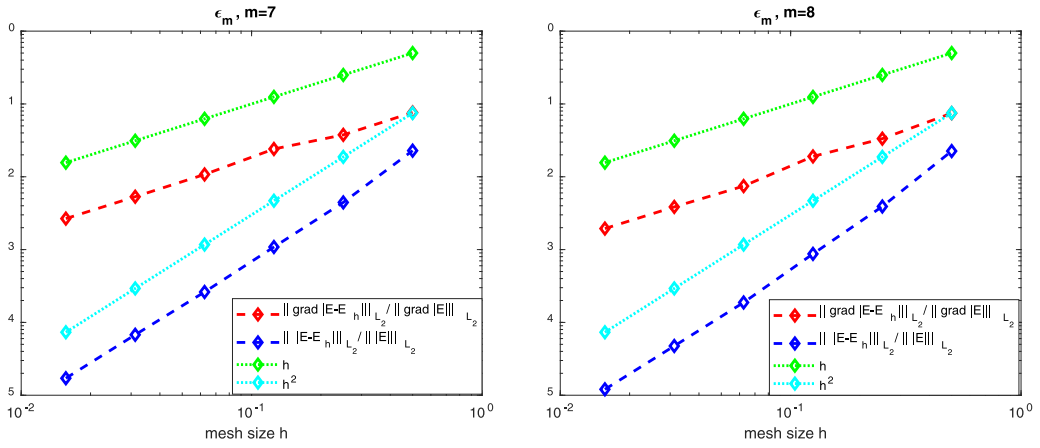

Fig. 5. Relative errors for $m = 7$ (left) and $m = 8$ (right).

7. Conclusion

In this paper we consider the time harmonic Maxwell's equations obtained through Laplace transform applied to a time-dependent model problem with a certain bounded, variable, and positive dielectric permittivity function $\varepsilon(x)$.

We construct a $P1$ stabilized finite element approximations for this problem and prove its consistency and well-posedness in a special case when the dielectric permittivity function has a constant value in a boundary neighborhood of the spacial domain. This problem is of vital importance in solving the *Coefficient Inverse Problems* (CIPs) [9] with several applications ranging from medical physics (radiation therapy) to micro turbines, computer chips, devices in fusion energy studies, etc.

As for the accuracy of the constructed numerical scheme we derive, optimal, a priori and a posteriori error bounds, in some, gradient dependent, weighted energy norms.

Finally, we have implemented several numerical examples that validate the robustness of the theoretical studies.

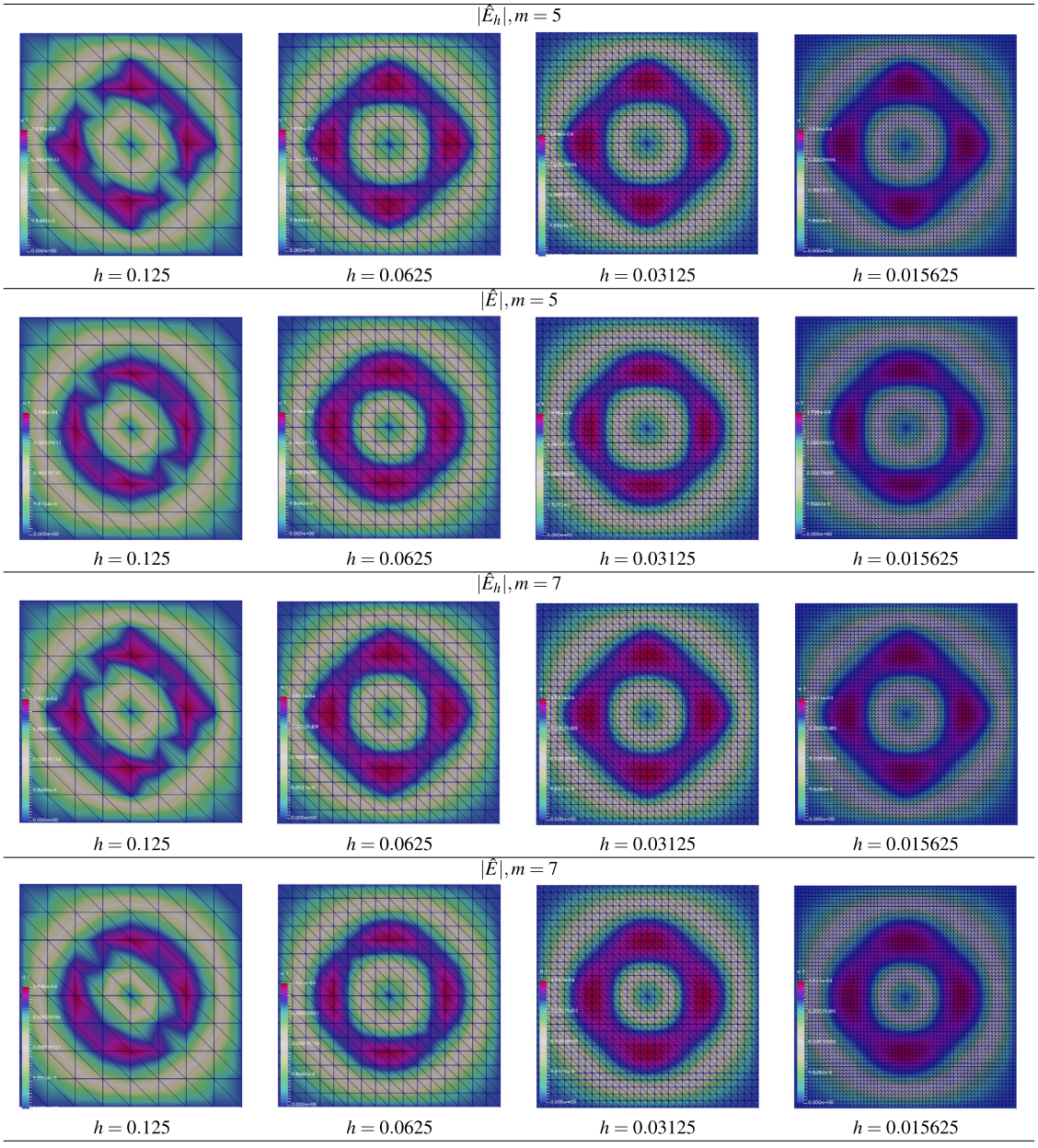

Fig. 6. Computed vs. exact solution for different meshes taking $m = 5$ and $m = 7$ in (6.51).

Acknowledgments

We are grateful to the unknown referee for the most careful review who pointed out shortcomings that contributed to the quality and improvement of our paper.

The research of both authors is supported by the Swedish Research Council, Sweden grant VR 2018-03661. The first author acknowledges the support of the Swedish Research Council (VR), Sweden grant DREAM.

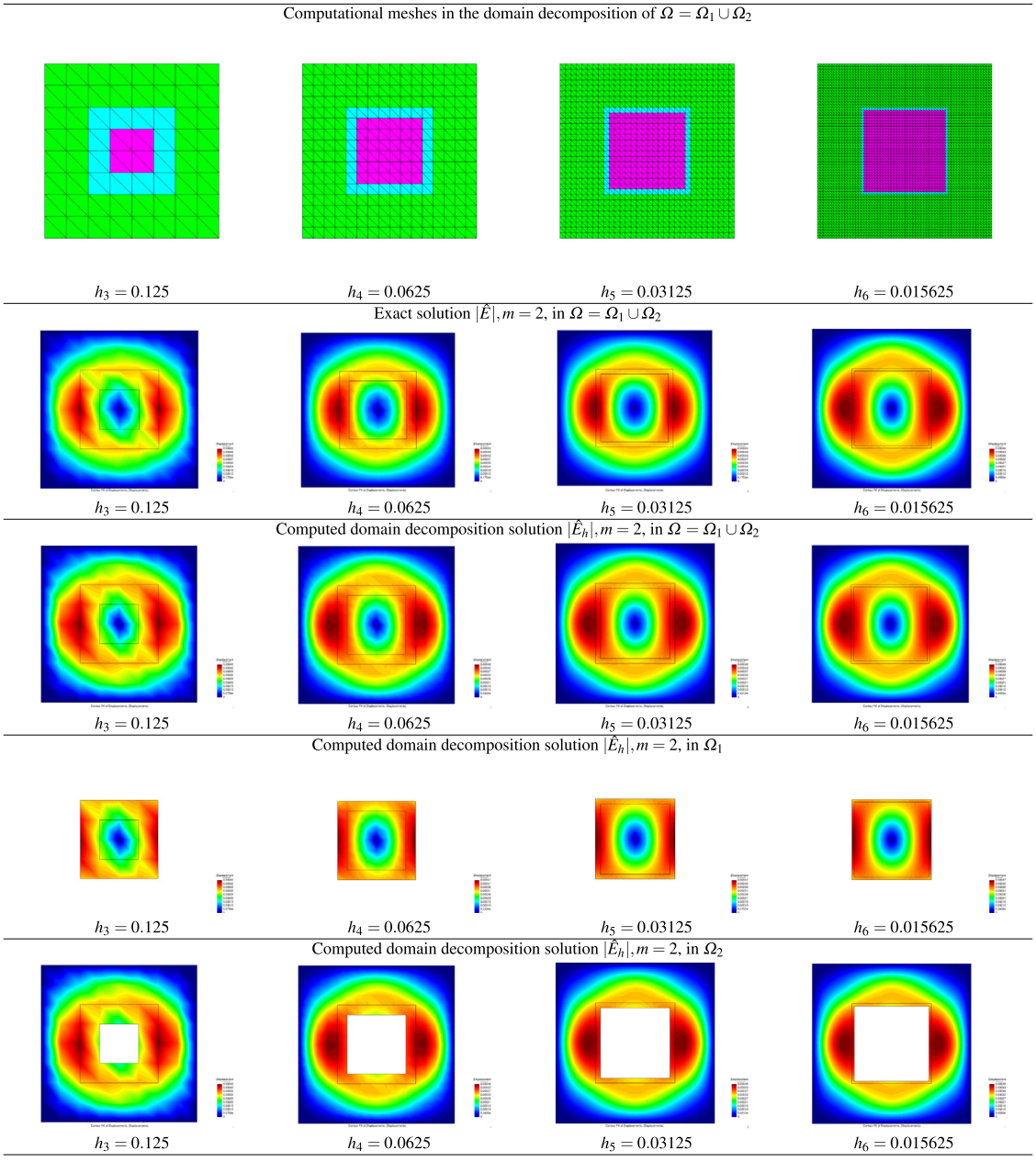

Fig. 7. Computed vs. exact solution for different meshes taking $m = 2$ in (6.51) using the Algorithm 1 in the domain decomposition method. Common boundaries between Ω_1 and Ω_2 are outlined by solid lines. Common nodes in Ω_1 and Ω_2 are in the domain outlined by light blue color. The computations are performed on four refined meshes $\mathcal{T}_{hl}$ with the mesh sizes $h_l = 2^{-l}, l = 3, 4, 5, 6$.

References

[1] Portable, Extensible Toolkit for Scientific Computation PETSc at http://.mcs.anl.gov/petsc/.
[2] Software package WavES at http://www.waves24.com/.
[3] Douglas N. Arnold, Franco Brezzi, Bernardo Cockburn, L. Dontella Marini, Unified analysis for discontinuous Galerkin methods for elliptic problems, SIAM J. Numer. Anal. 39 (5) (2002).
[4] M. Asadzadeh, An Introduction to Finite Element Methods for Differential Equations, Wiley, 2020.
[5] M. Asadzadeh, L. Beilina, On stabilized P1 finite element approximation for time harmonic Maxwell's equations, 2019, https://arxiv.org/abs/1906.02089.

[6] M. Asadzadeh, L. Beilina, Convergence of stabilized P1 finite element scheme for time harmonic Maxwell's equations, in: Springer Proceedings in Mathematics and Statistics, Vol. 328, Springer, Cham, 2020.
[7] F. Assous, P. Degond, E. Heinzé, P.-A. Raviart, J. Segré, On finite element method for solving the three-dimensional Maxwell equations, J. Comput. Phys. 109 (1993) 222–237.
[8] L. Beilina, Energy estimates and numerical verification of the stabilized domain decomposition finite element/finite difference approach for time-dependent Maxwell's system, Cent. Eur. J. Math. 11 (2013) 702–733, http://dx.doi.org/10.2478/s11533-013-0202-3.
[9] L. Beilina, M.V. Klibanov, Approximate Global Convergence and Adaptivity for Coefficient Inverse Problems, Springer, New York, 2012.
[10] L. Beilina, V. Ruas, An explicit P1 finite element scheme for Maxwell's equations with constant permittivity in a boundary neighborhood, arXiv:1808.10720.
[11] L. Beilina, V. Ruas, Convergence of explicit P1 finite-element solutions to Maxwell's equations, in: Springer Proceedings in Mathematics and Statistics, Vol. 328, Springer, Cham, 2020.
[12] L. Beilina, N.T. Th'anh, M.V. Klibanov, J.B. Malmberg, Globally convergent and adaptive finite element methods in imaging of buried objects from experimental backscattering radar measurements, J. Comput. Appl. Math. (2015) http://dx.doi.org/10.1016/j.cam.2014.11.055.
[13] J. Bondestam Malmberg, L. Beilina, An adaptive finite element method in quantitative reconstruction of small inclusions from limited observations, Appl. Math. Inf. Sci. 12 (1) (2018) 1–19.
[14] A.S. Bonnet-Ben Dhia, C. Hazard, S. Lohrengel, A singular field method for the solution of Maxwell's equations in polyhedral domains, SIAM J. Appl. Math. 59–6 (1999) 2028–2044.
[15] S.C. Brenner, L.R. Scott, The Mathematical Theory of Finite Element Methods, Springer-Verlag, Berlin, 1994.
[16] E. Burman, B. Stamm, Low order discontinuous Galerkin methods for second order elliptic problems, SIAM J. Numer. Anal. 47 (1) (2008/09) 508–533.
[17] E. Burman, B. Stamm, Local discontinuous Galerkin method with reduced stabilization for diffusion equation, Commun. Comput. Phys. 5 (2009) 498–524.
[18] P. Ciarlet Jr., Augmented formulations for solving Maxwell equations, Comput. Methods Appl. Mech. Engrg. 194 (2–5) (2005).
[19] P. Ciarlet Jr., E. Jamelot, Continuous Galerkin methods for solving the time-dependent Maxwell equations in 3D geometries, J. Comput. Phys. 226 (1) (2007).
[20] S. Cochez, S. Nicaise, Robust a posteriori error estimation for the Maxwell equations, Comp. Meth. Appl. Mech. Eng. 196 (2007).
[21] G.C. Cohen, Higher Order Numerical Methods for Transient Wave Equations, Springer-Verlag, Berlin, 2002.
[22] M. Costabel, A coercive bilinear form for Maxwell's equations, J. Math. Anal. Appl. 157 (2) (1991).
[23] M. Dauge, M. Costabel, Singularities of Maxwell's equations on polyhedral domains, in: M. Bach, C. Constanda, G.C. Hsiao, A.M. Sändig, P. Werner (Eds.), Analysis, Numerics and Applications of Differential and Integral Equations, in: Pitman Research Notes in Mathematics Series, Vol. 379, 1998.
[24] M. Dauge, M. Costabel, Weighted regularization of Maxwell equations in polyhedral domains. a rehabilitation of nodal finite elements, Numer. Math. 93 (2) (2002).
[25] V. Dolejsi, A. Ern, M. Vohralik, Hp-adaptation driven by polynomial-degree-robust a posteriori error estimates for elliptic problems, SIAM J. Sci. Comput. 38 (5) (2016).
[26] H. Egger, B. Radu, A second order finite element method with mass lumping for Maxwell's equations on tetrahedra, https://arxiv.org/abs/2002.05575.
[27] H. Egger, B. Radu, A mass-lumped mixed finite element method for Maxwell's equations, https://arxiv.org/abs/1810.06243.
[28] A. Elmkies, P. Joly, Finite elements and mass lumping for Maxwell's equations: the 2D case, Numerical Analysis, C. R. Acad. Sci. Paris 324 (1997) 1287–1293.
[29] B. Engquist, A. Majda, Absorbing boundary conditions for the numerical simulation of waves, Math. Comp. 31 (1977) 629–651.
[30] K. Eriksson, D. Estep, P. Hansbo, C. Johnson, Computational Differential Equations, Combridge, 1996.
[31] A. Ern, J.-L. Guermond, Finite element quasi-interpolation and best approximation, ESAIM Math. Mod. Numer. Anal. 51 (4) (2017).
[32] A. Ern, J.-L. Guermond, Analysis of the edge finite element approximation of the Maxwell equations with low regularity solutions, Comput. Math. Appl. 75 (3) (2018).
[33] P. Hansbo, M.G. Larson, Discontinuous Galerkin and the Crouzeix–Raviart element: application to elasticity, M2AN Math. Model. Numer. Anal. 37 (1) (2003) 63–72.
[34] E. Jamelot, Résolution des équations de Maxwell avec des éléments finis de Galerkin continus, (Ph.D. thesis), Ecole Polytechnique, 2005.
[35] B. Jiang, The Least-Squares Finite Element Method. Theory and Applications in Computational Fluid Dynamics and Electromagnetics, Springer-Verlag, Heidelberg, 1998.
[36] B. Jiang, J. Wu, L.A. Povinelli, The origin of spurious solutions in computational electromagnetics, J. Comput. Phys. 125 (1996) 104–123.
[37] J. Jin, The Finite Element Method in Electromagnetics, Wiley, 1993.
[38] C. Johnson, Numerical Solutions of Partial Differential Equations By the Finite Element Method, Studentlitteratur, 1987.
[39] P. Joly, Variational methods for time-dependent wave propagation problems, in: Lecture Notes in Computational Science and Engineering, Springer, 2003.
[40] P.B. Monk, Finite Element Methods for Maxwell's Equations, Oxford University Press, 2003.
[41] P.B. Monk, A.K. Parrott, A dispersion analysis of finite element methods for Maxwell's equations, SIAM J. Sci. Comput. 15 (1994) 916–937.

[42] C.D. Munz, P. Omnes, R. Schneider, E. Sonnendrucker, U. Voss, Divergence correction techniques for Maxwell Solvers based on a hyperbolic model, J. Comput. Phys. 161 (2000) 484–511.
[43] J.-C. Nédélec, Mixed finite elements in R3, Numer. Math. 35 (1980) 315–341.
[44] K.D. Paulsen, D.R. Lynch, Elimination of vector parasites in Finite Element Maxwell solutions, IEEE Trans. Microw. Theory Technol. 39 (1991) 395–404.
[45] Daniel Antonio Di Pietro, Alexandre Ern, Mathematical Aspects of Discontinuous Galerkin Methods, Mathematiques et Applications, Vol. 69, Springer, 2012.
[46] V. Ruas, M.A. Silva Ramos, A Hermite method for Maxwell's equations, Appl. Math. Inf. Sci. 12–2 (2018) 271–283.
[47] J. Schöberl, A posteriori error estimates for Maxwell equations, Math. Comp. 77 (262) (2008).
[48] N.T. Thánh, L. Beilina, M.V. Klibanov, M.A. Fiddy, Reconstruction of the refractive index from experimental backscattering data using a globally convergent inverse method, SIAM J. Sci. Comput. 36 (2014) B273–B293.
[49] N.T. Thánh, L. Beilina, M.V. Klibanov, M.A. Fiddy, Imaging of buried objects from experimental backscattering time-dependent measurements using a globally convergent inverse algorithm, SIAM J. Imaging Sci. 8 (1) (2015) 757–786.